Using Light as a Lens for Submicron, Neutral-Atom Lithography

G. Timp, R. E. Behringer, D. M. Tennant, and J. E. Cunningham

AT&T Bell Laboratories, Holmdel, New Jersey 07733

M. Prentiss and K. K. Berggren

Harvard University, Cambridge, Massachusetts 02138

We show that light can be used as a lens to focus a collimated neutral atomic beam to submicron dimensions during deposition onto a substrate. We have used an optical standing wave at 589 nm as an array of cylindrical lenses to focus a perpendicular sodium beam into a grating on a substrate, with a periodicity of 294.3 ± 0.3 nm. This result is the first direct evidence of submicron focusing of atoms by light, and represents a fundamentally new scheme for submicron lithography.

We present here a new scheme for submicron lithography that uses the force exerted by light to deflect a neutral atomic beam during deposition onto a substrate. For a stationary, two-level atom, the average stimulated force exerted by nearly resonant light is proportional to the intensity gradient [1,2]. In a standing wave (SW), the intensity oscillates spatially every half wavelength, and the corresponding oscillations in the average force on an atom can be used as an array of weak cylindrical lenses. If the frequency of the SW is detuned above (below) the two-level resonance, the atoms are attracted toward the intensity nodes (antinodes). Semiclassically, collimated atoms are narrowly distributed about the nodes, analogous to the focusing of parallel rays of light passing through an array of cylindrical lenses [3].

In this Letter we demonstrate that a SW at 589 nm, interacting with a collimated atomic sodium beam, can be used to make a regular grating over approximately a 0.2-cm^2 area on a silicon substrate, with a 294.3 ± 0.3-nm period. Our calculations show that the gradient force may be capable of producing features on a 10-nm scale every half wavelength. The predicted small feature size results from the nearly linear position dependence of the force on a neutral atom near the nodes (antinodes) of an optical SW for positive (negative) detuning.

This result not only represents a new scheme for submicron lithography, but it is also the first direct evidence of optical focusing of atoms on a submicron scale. There have been indirect measurements of the nonuniform density that results when atoms interact with a SW [4,5], but these measurements examined net average distributions over large volumes (~ 1 cm^3) and were not able to determine the submicron regularity of the density variations. This issue is especially relevant because atoms trapped by a three-dimensional SW are known to exhibit variations in optical density on the scale of at least 100 μm [5].

Figure 1 is a schematic of the experiment. A collimated sodium atomic beam, propagating along $\hat{y}$, interacts with a perpendicular SW. The SW intensity is uniform over a distance of L_i ($=300$ μm typically) along $\hat{y}$ but vanishes elsewhere. The wave vector of the SW is $|k|\hat{z} = (2\pi/\lambda)\hat{z}$, where $\lambda = 589$ nm is the optical wave-

length. The atoms in the sodium beam have an average velocity along $\hat{y}$ of v_y ($=740$ m/s typically), and interact with the SW for a time $t_i = L_i/v_y$ (<0.5 μs typically). After emerging from the SW, a sodium atom undergoes free flight for a distance L_{ff} before it hits the substrate; i.e., there are no forces acting on the atom in the interval L_{ff} because there is no light beyond L_i.

The average force exerted by a SW on a two-level atom with negligible transverse velocity (i.e., $v_z, v_x \approx 0$) is derived from the gradient of the pseudopotential:

$$U(z) = \tfrac{1}{2} \hbar \Delta \ln[1 + 2\omega_R^2(z)/(4\Delta^2 + \Gamma^2)], \quad (1)$$

where $\Delta = \omega_L - \Omega$ is the detuning between the laser (ω_L) and the atomic frequency (Ω), Γ is the natural lifetime of the resonance, and $\omega_R(z) = \mu E(z)/2\hbar$ is the local Rabi frequency, proportional to the product of the dipole moment, μ, and the electric field, $E \sim \sin[kz]$. Thus, the periodic variation in the square of the Rabi frequency gives rise to a potential that is periodic in $\lambda/2$. Typically, the depth of the potential is about 5 μeV. For the pseudopotential approximation to be valid, a few (1-2) spontaneous emission lifetimes Γ^{-1} must elapse before the atoms can come to equilibrium with the light field [6].
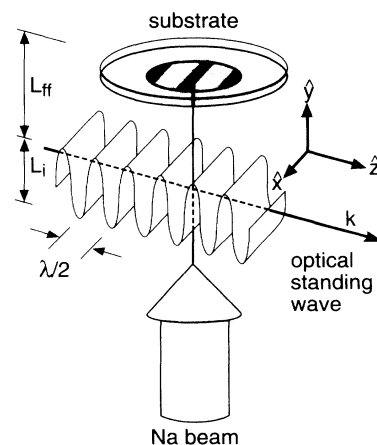

FIG. 1. A schematic representation of the experiment. An optical standing wave is interposed between an atomic beam and a substrate to deflect atoms during deposition.

Thus, t_i (and L_i) are uncertain to within the time for spontaneous emission. [Typically, $t_i \approx (5-20) \times \Gamma^{-1}$.]

$U(z)$ acts as an array of weak cylindrical lenses, focusing the atomic beam into a grating on the substrate, with a period of $\lambda/2$. If the potential within each half wavelength of the SW was harmonic with an oscillation period T (typically 0.5 μs) then, when $t_i = T/4$, a perfectly collimated monoenergetic atomic beam would be focused to an array of lines in which each line would have a delta-function distribution along $\hat{z}$ for $L_{ff}=0$. Actually, spherical aberrations associated with deviations from the harmonic potential, chromatic aberrations associated with the finite atomic energy spread, diffusive aberrations associated with random fluctuations in the spontaneous and gradient forces, and diffraction aberrations due to the atomic wavelength and $L_{ff} \neq 0$ contribute to the finite width of the distribution. Semiclassical calculations of the atomic trajectories (see below) that account for the spherical and chromatic aberrations show the linewidth can be about 10 nm. Diffusive aberrations [7], diffraction, and the de Broglie wavelength are estimated [1] to be of this order also, but are ignored in our analysis.

For an atomic beam with a practical deposition rate (typically 0.1–0.01 nm/s), the initial kinetic energy associated with v_z can be substantial compared to $|U|$. In our experiments the sodium beam emanates from a 5-g glass ampoule, heated to approximately 225 °C. Because the stem of the ampoule was 7 cm long with a 3.5-mm inside radius, the sodium beam was partially collimated about the $\hat{y}$ direction with approximately a 50-mrad angular divergence corresponding to a transverse velocity spread along $\hat{z}$ less than approximately ± 40 m/s.

To reduce the transverse velocity, we use "Doppler" optical molasses (MO) [8] to cool the atomic beam along $\hat{z}$ before it interacts with the SW. The MO is especially effective at cooling velocities within the range $|v_z| < 2\pi\Delta/k \approx 30$ m/s. The optics associated with the MO and SW are shown in Fig. 2. The laser source is a single Coherent 899 tunable dye laser. The laser frequency is nearly resonant with the sodium $3^2S_{1/2} \rightarrow 3^2P_{3/2}$ transition that has a linewidth of $\Gamma/2\pi = 10$ MHz. The MO and SW were formed by retroreflecting two separate incoming traveling waves (TW) off a single mirror, M1, mounted on a piezoelectric transducer (PZT).

The MO has two frequency components. The first component is detuned 30–40 MHz below the transition between the $F=2$ sublevel of the ground state (GS) and the $F=3$ sublevel of the excited state (ES) and has an intensity of 30 mW/cm^2 in each TW. The second component is tuned to the transition between the $F=1$ GS sublevel and the $F=2$ ES sublevel and has an intensity of 10 mW/cm^2 in each TW. All four TWs have uniform intensity across an ≈ 1-cm-diam spot and are circularly polarized with respect to the 10-G magnetic field oriented in the $\hat{z}$ direction. The two frequency components and the magnetic field are present to prevent optical pumping [9].
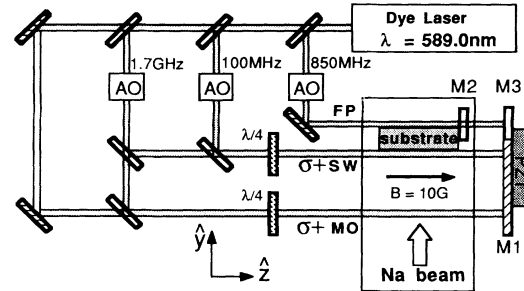

FIG. 2. A detailed schematic of the optical apparatus used to generate the standing wave (SW), the optical molasses (MO), and the Fabry-Pérot resonator (FP). The $\lambda/4$ plates are used to change the polarization of the light. The $F=1$ and $F=2$ ground-state sublevels of Na are split by 1.7 GHz. The 1.7-GHz acousto-optic modulator (AO) shifts the laser frequency to avoid optical pumping. The 100-MHz AO shifts the laser to detune the SW, and the 850-MHz AO permits the frequency modulation of the FP resonator.

Emerging from the MO, the atomic beam then interacts with the SW, which is uniform in intensity with a width of ≈ 1 mm along $\hat{x}$ and 250–500 μm along $\hat{y}$. The SW is clipped along $\hat{y}$ by the edge of a 2-cm square silicon substrate so that L_{ff} is minimized ($L_{ff} < 10$ μm). ($L_{ff} \neq 0$ even if the substrate is not intentionally tilted because of misorientation and substrate flatness.) The SW also has two frequency components. The first component, detuned Δ from the transition between the $F=2$ GS and the $F=3$ ES, is varied between experiments. The intensity in this component is approximately 5 W/cm^2 for each TW. The second component, tuned to the $F=1$ GS to the $F=2$ GS transition, has about 500 mW/cm^2 in each TW. The latter component prevents optical pumping.

Mechanical vibrations of the substrate relative to the position of the SW minima can smear the lines that compromise the grating. Thus, it is crucial that the $\hat{z}$ coordinates of the SW nodes remain fixed relative to the substrate during the 10-min deposition. We stabilize the position of the SW node at M1 using a Fabry-Pérot resonator (FP). The PZT, which holds M1, also supports a partially reflecting mirror, M2. The FP is made using M2 and a second partially reflecting mirror M3 mounted onto the brass block holding the substrate. The positions of M1 and M2 are adjusted via the PZT so that the FP is resonant. The stabilization was done using an ac detection scheme in which a 40-kHz frequency was impressed on the light used for the FP by modulating the frequency of the 850-MHz AO. This insured that the distance between the brass block holding the substrate and M1 was an integral multiple of the $\lambda/2$. The SW nodes remained fixed relative to the substrate within $\lambda/45 \approx 13$ nm.

We used first-order optical diffraction to investigate *in situ* the region where the film has been modified by the SW. Figure 3 is a schematic representation of the diffraction geometry. An incident beam with 560 nm $< \lambda < 580$ nm at an angle in the range $8° < \theta_i < 15°$
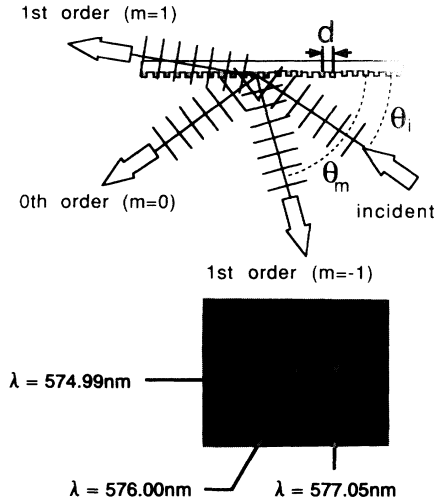
FIG. 3. A schematic of the diffraction geometry used to detect the grating and a photograph of three $m = -1$ diffraction spots obtained using this geometry for three different incident wavelengths on the grating.

from the surface backscatters at $6° < \theta_m < 17°$. According to

$$-d(\cos\theta_m + \cos\theta_i) = m\lambda , \qquad (2)$$

we observe the first-order, $m = -1$, diffraction peak. In Eq. (2), θ_i is the angle between the surface and the incident wave vector, θ_m is the angle between the surface and the diffracted light, and d is the grating period. We observe diffraction only over the area associated with the position of the SW. In correspondence with Eq. (2), the diffraction depends on the incident wavelength. Figure 3 also shows a photograph of three $m = -1$ diffraction peaks corresponding to three different incident wavelengths: 574.99, 576.00, and 577.05 nm. The photograph was obtained with the diffraction geometry shown in the top part of Fig. 3 using three different exposures at the same position for the three wavelengths. The diffraction spots are separated by about 7 mm and were observed approximately 40 cm from the grating for $\theta_i \approx 10°$ and $\theta_m \approx 13°$.

We measured d at a variety of wavelengths and angles. For example, using the condition $\theta_i = -\theta_m = 11.56°$ when $\lambda = 577.05$ nm, we found $d = 294.3 \pm 0.3$ nm independent of the detuning and intensity in the SW (see Table I). We also measured the diffraction efficiency, i.e., the ratio, η, of the intensity found in the $m = -1$ diffraction peak to the incident intensity, and found a weak dependence on the detuning and the power in the SW. The largest η we found is less than 0.04%. Table I summarizes our observations of the period and the diffraction efficiency obtained from the $m = -1$ diffraction peak as a function of the detuning and Rabi frequency.

The fidelity of a grating made using a SW at $\Delta = 70$ MHz and $\omega_R = 100$ MHz was evaluated from the angular

TABLE I. A list of the measured parameters for gratings made with a SW and conventional EB lithography. The parameters are defined in the text. Typically $L_i = 250$ μm; $L_{ff} < 10$ μm.

Δ (MHz)	ω_R (MHz)	d (nm)	$10^4\eta$
+70	150	294.1 ± 1.0	1.5 ± 0.5
+70	100	294.3 ± 0.3	4.0 ± 1.0
+70	80	294.1 ± 0.5	$\cdots$
−130	100	294.5 ± 0.8	2.0 ± 0.5
AuPd/PMMA EB grating	$\cdots$	300.6 ± 2.0	33 ± 0.5

width of the $m = -1$ diffraction peak. Figure 4(a) shows the $m = -1$ diffraction spot found 42 cm from a grating with 577.05-nm light incident at $\theta_i \approx 10°$ using an incident beam 100 μm wide. The spot has an angular width of approximately 4×10^{-3} rad. This width corresponds to a spot $\approx (100 \ \mu m)^{-1}$ wide. Thus, the width of the spot is limited by the 100-μm portion of the grating that is illuminated, and so we deduce that the grating is regular over at least that scale. For comparison, we show in Fig. 4(b) the diffraction from a nominal 300-nm-period grating, 100 μm on edge, fabricated using conventional electron beam lithography (EB). The diffraction pattern of Fig. 4(b) was obtained at $\lambda = 587.8$ nm under the same conditions as Fig. 4(a). The EB grating was made in 80-nm-thick polymethylmethacrylate (PMMA) resist; after exposure and development, a 50-nm-thick layer of AuPd was deposited onto the grating in the PMMA. The EB grating was comprised of sharp lines and spaces approximately 150 nm wide. With $\theta_i = -\theta_m = 11.5°$, we found that $d = 300.6 \pm 1.0$ nm for the EB grating. The additional oscillations found in the diffraction pattern from the EB grating of Fig. 4(b) are evi-
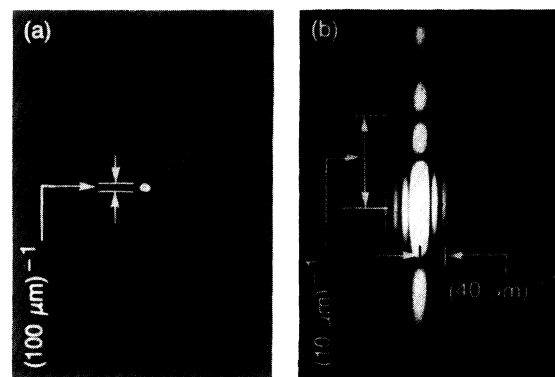

FIG. 4. (a) The $m = -1$ diffraction spot obtained from a grating made with an optical standing wave. The diffraction was obtained with $\lambda = 577.05$ nm light using an incident beam focused to 100 μm. The $(100 \ \mu m)^{-1}$ width of the peak is indicative of the fidelity and regularity of the grating. (b) The $m = -1$ diffraction spot obtained from a grating made using conventional EB lithography. The diffraction was obtained with $\lambda = 587.80$ nm under the same conditions and using the same angles as in (a).
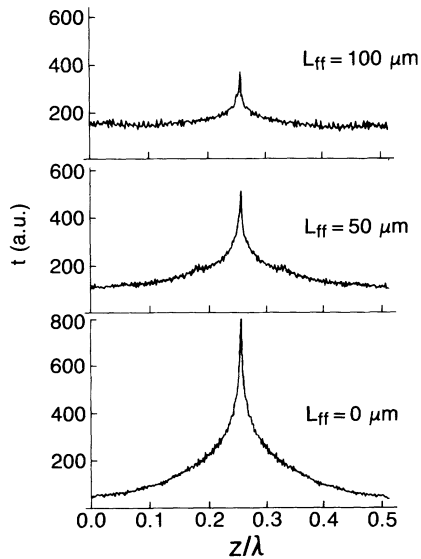
FIG. 5. Semiclassical numerical simulations showing the thickness profile of the film over a half wavelength field for free flight gaps, $L_{ff}=0$, 50, and 100 μm when $\Delta=-150$ MHz, $\omega_R=100$ MHz, and $L_i=250$ μm.

dence of the 100-μm spatial field size and of smaller ≈ 5 μm $\times 10$ μm area irregularities in the grating. Figure 4(b) is typical of diffraction obtained from four EB gratings. We measured $\eta=3.3\times10^{-3}$ for the EB grating, which is 10 times larger than that observed on gratings made with a SW. We cannot attribute the difference in η unequivocally to the width of the lines which comprise the respective gratings, however, because of differences in materials, grain size, etc.

Finally, we attempted to evaluate the depth of focus for a thermal atomic beam by measuring the diffraction efficiency of gratings made using a SW as a function of L_{ff}. To change L_{ff} we intentionally tilted the substrate along $\hat{z}$ relative to the SW and allowed the SW to touch one edge (the right-hand edge) of the substrate. In one experiment, we tilted the substrate about $0.4°$ relative to the SW. For $\Delta=-130$ MHz, $\omega_R=100$ MHz, $L_i \approx 250$–500 μm we found a diffraction spot when $L_{ff}<10$ μm, i.e., near the right-hand edge. As a function of position along the substrate, L_{ff} increased from zero at the right-hand edge to approximately 200 μm at the opposite edge, but $m=-1$ diffraction could not be observed for $L_{ff}>50$ μm. When the substrate is tilted at either $0.05°$ or $1.9°$ relative to the SW, we found that the diffraction was generally extinguished beyond $L_{ff}>50\pm15$ μm.

This observation is in correspondence with semiclassical numerical simulations of the film profile. Figure 5 illustrates the effect of a gap between the SW and the substrate corresponding to the experimental conditions. In Fig. 5 the variation in the film thickness, t, is plotted over $0<z<\lambda/2$ for $L_{ff}=0$, 50, and 100 μm. To calculate the results of Fig. 5 we assume the atoms initially have a uniform spatial distribution along $\hat{z}$, with $v_z=0$ and a

Boltzmann velocity distribution along $\hat{y}$. We suppose that the atoms are fully polarized the instant they enter the SW, and we numerically calculate their trajectories using the force associated with Eq. (1). Thus, chromatic and spherical aberrations are included implicitly. The atomic coordinates of between 10000 and 100000 two-level atoms are updated every 100 ps. The numerical resolution of the final position of the atoms on the substrate is 0.3–1 nm. We assume that there is no diffusion once the atom hits the substrate, and we ignore any mechanical vibrations of the substrate relative to the SW.

The narrow peak found near $z=\lambda/4$ for $L_{ff}=0$ in Fig. 5 is approximately 10 nm wide (FWHM), and is indicative of the focusing that can be achieved for particular longitudinal velocities in the Boltzmann distribution. (The width of the lines in the gratings that we actually made are larger than 10 nm because of mechanical vibration, surface diffusion, and aberrations not accounted for in the simulation.) The background surrounding the peak corresponds to the chromatic aberrations associated with the remaining velocity groups in the Boltzmann distribution, and to spherical aberrations associated with atoms that have initial z positions outside the range where the potential is harmonic. We find that as L_{ff} increases, higher velocity atoms in the Boltzmann distribution are focused because of chromatic aberration, but there are fewer of them. Thus, the narrow peak near $z=\lambda/4$ has about the same width as a function of L_{ff}, but a different height relative to the background. According to the simulation, we estimate that for an increase in L_{ff} from 0 to 100 μm, the relative η will fall by at least a factor of 10 in qualitative agreement with our observations.

[1] J. P. Gordon and A. Ashkin, Phys. Rev. A 21, 1606 (1980).

[2] J. E. Bjorkholm et al., Phys. Rev. Lett. 41, 1361 (1978).

[3] In contrast with work by P. E. Moskowitz et al. [Phys. Rev. Lett. 51, 370 (1983)] and by O. Carnal et al. [Phys. Rev. Lett. 67, 3231 (1991)], quantum-mechanical focusing is negligible under our experimental conditions.

[4] C. Salomon et al., Phys. Rev. Lett. 59, 1659 (1987).

[5] N. P. Bigelow and M. G. Prentiss, Phys. Rev. Lett. 65, 28 (1990).

[6] Y. Castin, J. Dalibard, and C. Cohn-Tannoujdi, in LIKE Proceedings, Elba, May, 1990 (to be published).

[7] The diffusive aberrations associated with force fluctuations are small because for short t_i the diffusion is faster in velocity space than in real space. We have simulated the effect of fluctuations using our experimental parameters and a spatially independent diffusion coefficient of 10^{-45} in SI units (the maximum value [1] that should occur within $\lambda/2$) and find a linewidth broadened by 4 nm.

[8] S. Chu et al., Phys. Rev. Lett. 55, 48 (1985).

[9] W. D. Phillips, J. V. Prodan, and H. J. Metcalf, J. Opt. Soc. Am. 2, 1751 (1985).
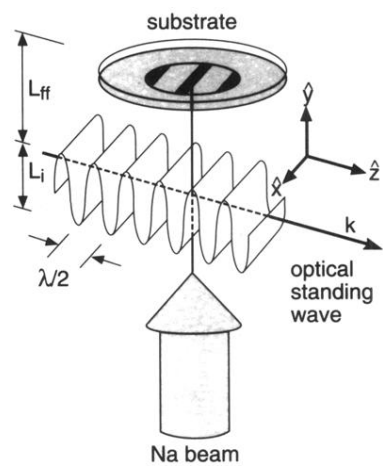
FIG. 1. A schematic representation of the experiment. An optical standing wave is interposed between an atomic beam and a substrate to deflect atoms during deposition.
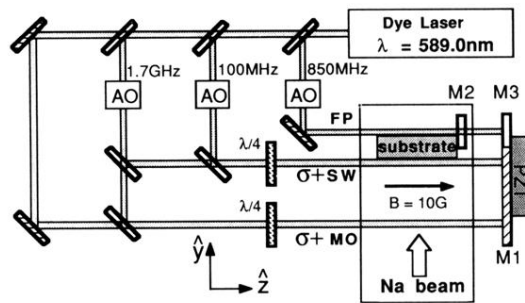
FIG. 2. A detailed schematic of the optical apparatus used to generate the standing wave (SW), the optical molasses (MO), and the Fabry-Pérot resonator (FP). The $\lambda/4$ plates are used to change the polarization of the light. The $F=1$ and $F=2$ ground-state sublevels of Na are split by 1.7 GHz. The 1.7-GHz acousto-optic modulator (AO) shifts the laser frequency to avoid optical pumping. The 100-MHz AO shifts the laser to detune the SW, and the 850-MHz AO permits the frequency modulation of the FP resonator.

1st order (m=1)

d

θ_i

0th order (m=0)

θ_m

incident

1st order (m=-1)

$\lambda = 574.99\text{nm}$

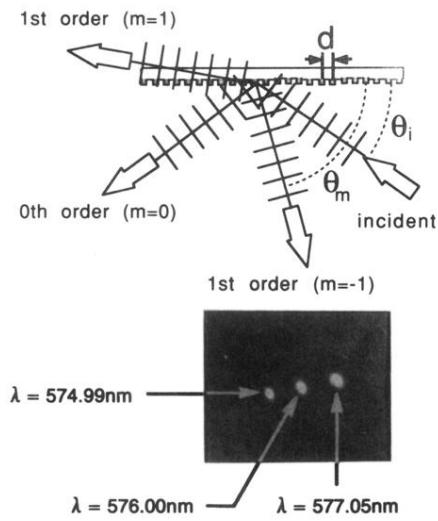$\lambda = 576.00\text{nm}$

$\lambda = 577.05\text{nm}$

FIG. 3. A schematic of the diffraction geometry used to detect the grating and a photograph of three $m = -1$ diffraction spots obtained using this geometry for three different incident wavelengths on the grating.
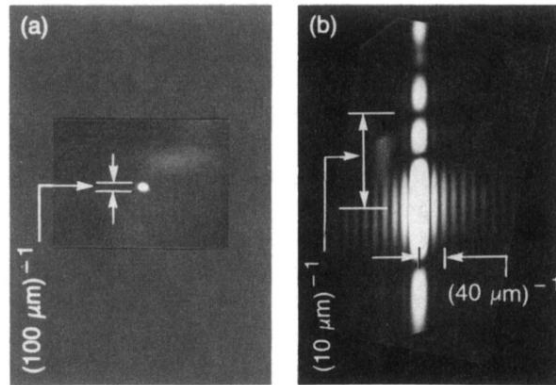
FIG. 4. (a) The $m = -1$ diffraction spot obtained from a grating made with an optical standing wave. The diffraction was obtained with $\lambda = 577.05$ nm light using an incident beam focused to 100 μm. The $(100\ \mu m)^{-1}$ width of the peak is indicative of the fidelity and regularity of the grating. (b) The $m = -1$ diffraction spot obtained from a grating made using conventional EB lithography. The diffraction was obtained with $\lambda = 587.80$ nm under the same conditions and using the same angles as in (a).